Journal of Electronic Imaging

JElectronicImaging.org

Effect of pupil dilation on off-angle iris recognition

Mahmut Karakaya
Elif T. Celik

SPIE. IS&T imaging.org

Mahmut Karakaya, Elif T. Celik, "Effect of pupil dilation on off-angle iris recognition," *J. Electron. Imaging* **28**(3), 033022 (2019), doi: 10.1117/1.JEI.28.3.033022.

Journal of Electronic Imaging 28(3), 033022 (May/Jun 2019)

Effect of pupil dilation on off-angle iris recognition

Mahmut Karakaya[a,*] and Elif T. Celik[b]
[a]University of Central Arkansas, Department of Computer Science, Conway, Arkansas, United States
[b]University of South-East Europe-LUMINA, Faculty of Engineering Sciences, Bucharest, Romania

Abstract. Due to the less constrained setup in standoff iris recognition systems, it is likely to capture nonideal iris images with gaze angle, pupil dilation, reflections, and occlusions. The combined effect of pupil dilation and gaze angle on iris recognition is examined. We first highlight the effects on synthetic images generated with a biometric eye model using a ray-tracing algorithm. Then, we quantify the effects of pupil dilation and gaze angle on the real frontal and off-angle images at different dilation levels. Our experiments reveal that the larger differences in dilation levels and gaze angles between the compared iris images increase the Hamming distance. Even if the linear rubber-sheet normalization helps to minimize the dilation effect in frontal images, it cannot fully eliminate it in off-angle iris images because of not only the pupil dilation and three-dimensional iris texture but also the corneal refraction distortion and limbus occlusion. We also observe that the gaze angle is the main reason for the performance degradation in steeper off-angle images, where the effect of the dilation is limited. In addition, since the iris region in off-angle and dilated iris images is smaller than that in frontal and constricted iris images, their interclass Hamming distance distribution is shifted toward the intraclass distribution, which may increase the false match rate. [DOI: 10.1117/1.JEI.28.3.033022]

Keywords: biometrics; iris recognition; pupil dilation; off-angle iris images.

Paper 190043 received Jan. 15, 2019; accepted for publication May 13, 2019; published online Jun. 5, 2019.

1 Introduction

Due to its accuracy, reliability, and distinctness, iris recognition is known as one of the best biometric solutions for identification and verification in different applications ranging from airports to hospitals.[1] A traditional iris recognition system is designed to recognize individuals standing in front of a well-controlled imaging system by following five steps, namely data acquisition, segmentation, normalization, encoding, and matching, as shown in Fig. 1. After illuminating the eye using near-infrared light, the iris image is captured with a near-infrared–sensitive camera. Then, the iris region is extracted from its surroundings by segmenting its inner (pupil) and outer (sclera) boundaries. The normalization step transforms the segmented circular iris texture into a rectangular shape using a pseudopolar co-ordinate system. This unwrapped iris image is converted to a binary iris code using Gabor filters. In the final matching step, the similarity between an iris code and previously enrolled iris codes in a database is determined by calculating their Hamming distances. The Hamming distance is a ratio of the number of different bits between two compared binary iris codes to a total number of compared bits. The comparison of iris codes from the same subject generates intraclass Hamming distance, where the expected score is close to zero. Iris codes from different individuals have a 0.5 Hamming distance that is called interclass comparison. Therefore, if the Hamming distance between two irises is less than a predefined threshold, it is accepted that they belong to the same eye or otherwise.

Recent improvements in imaging and computation technologies have enabled us to design standoff biometric systems to recognize not only the cooperative users but also the noncooperative individuals during their motion. Due to the less constrained setup in standoff systems compared with traditional iris recognition systems, a standoff system is more likely to capture nonideal iris images with gaze angle, pupil dilation, reflections, and occlusions. Although traditional iris recognition algorithms[2–6] have shown excellent recognition performance in the past decade to recognize ideal iris images captured from cooperative users, their accuracy is highly correlated with the image quality and similarity of imaging condition. Therefore, standoff iris recognition is an emerging research area that requires updating the traditional algorithms to recognize the nonideal images that captured both cooperative and noncooperative individuals.

For example, comparing iris images captured from different angles degrades the recognition performance not only because of perspective distortion but also the effects of different eye structures, including the cornea, limbus, sclera, aqueous humor, iris, and lens. The appearance of the iris in the captured standoff image depends on the image acquisition angle because of corneal refraction, complex iris texture, limbus occlusion, lens accommodation, and depth of field blur. First, the incoming and outgoing light rays are refracted in the cornea and aqueous humor with respect to the gaze angle. Second, the limbus, a semitransparent structure at the intersection of the cornea and sclera, occludes part of the iris plane depending on the acquisition angle. Third, since the iris has three-dimensional (3-D) texture, its appearance differs with respect to angle, it presents shadows, and part of the iris is blurred due to leaving the depth of camera focus. Fourth, lens changes the curvature of the iris surface during the accommodation of the eye. Finally, the combination of these challenging effects has a more significant negative impact on recognition accuracy. Especially, steeper gaze angles require additional efforts to eliminate these challenging effects. Detailed information regarding the effect of

*Address all correspondence to Mahmut Karakaya, E-mail: mkarakaya@uca.edu

1017-9909/2019/$25.00

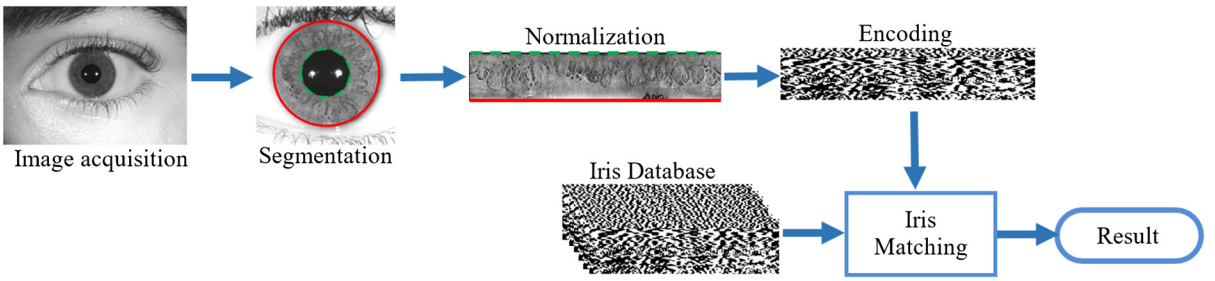

Fig. 1 Flow chart of a traditional iris recognition system.

eye structures on off-angle iris recognition can be found in our previous study.[7]

Examples of frontal and off-angle images of the same iris with dilated and constricted pupils are shown in Fig. 2, where their acquisition angles are 0 deg and 40 deg, respectively. Frontal constricted and dilated iris images in Figs. 2(a)–2(b) have an obvious texture difference due to pupil dilation. The effect of corneal refraction and limbus occlusion can be easily seen between frontal and off-angle iris images, as shown in Figs. 1(a) and 1(c), because of the difference in gaze angle even if they have the same pupil dilation. The comparisons of iris images in Figs. 2(a) and 2(d) or Figs. 2(b) and 2(c) are examples of the combined effect of gaze angle and pupil dilation on the appearance of the iris texture. Traditional iris recognition algorithms give a false reject for the comparison of these images.

In this paper, we study the combined effect of pupil dilation and gaze angle on the accuracy of iris recognition systems. In Sec. 2, an overview of previous studies on standoff iris recognition is provided. Section 3 presents the effect of pupil dilation on the performance of iris recognition using a biometric eye model with circular patterns at different dilation levels. Experimental setup and dataset are presented at Sec. 4. Section 5 presents experimental results and discussions. Finally, we conclude in Sec. 6 and provide possible future works.

2 Related Works for Standoff Iris Recognition

In biometrics literature, there are only a few related works that handle the challenging issues in standoff iris recognition systems. Daugman,[5] Schuckers et al.,[6] Zuo et al.,[8] and Li et al.[9] proposed some methods to improve the recognition performance. However, their approaches, such as affine transformations, elliptical normalization, and perspective transformation, only focus on geometric distortion and ignore other challenging issues in standoff images, including corneal refraction, complex 3-D iris textures, depth-of-blur, limbus occlusion, and pupil dilation. Although they showed some improvements on the accuracy of off-angle iris images, their performance drops dramatically beyond 30 deg in angle. Price et al.,[10] Frigerio et al.,[11] and Santos-Villalobos et al.[12] focused on corneal refraction effect in off-angle iris images. Although their methods also showed some improvements with synthetic off-angle images, they noted that the

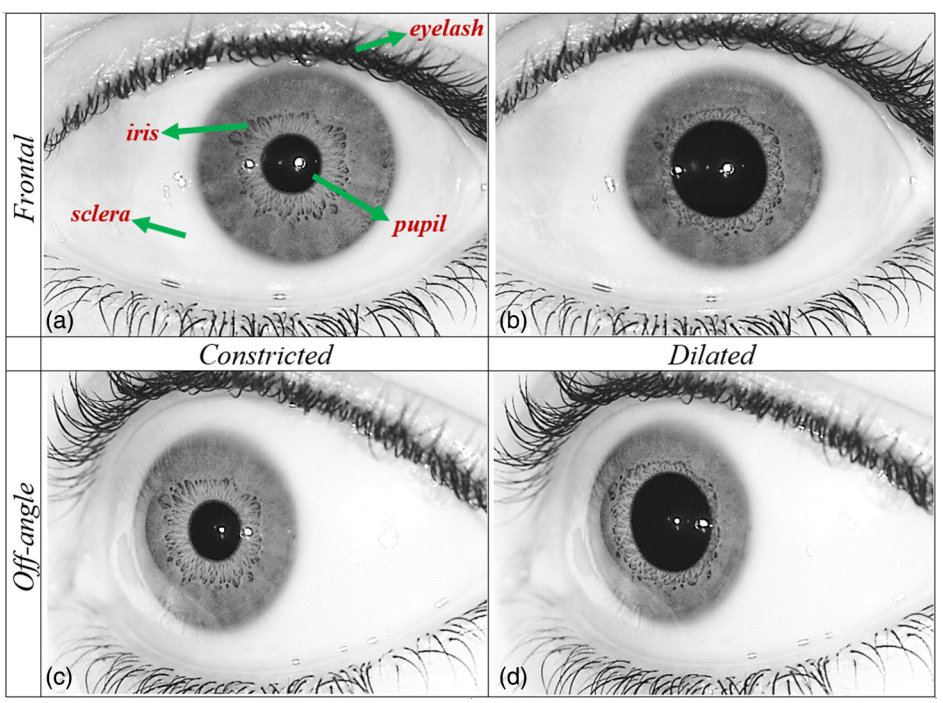

Fig. 2 Examples of iris images from (a, b) 0 deg in angle (frontal) and (c, d) 40 deg in angle (off-angle). Note that panels (a, c) and (b, d) have the same dilation levels.

main obstacle is a lack of a complete solution for real off-angle iris images. Karakaya et al.[13] investigated the limbus effect on off-angle iris images and showed that the limbus effect degrades the accuracy of stand-off iris recognition significantly.

The influence of the change of the pupil size (dilation/contraction) is another active research topic both in traditional and standoff recognition systems. There are some pioneering studies examining the effects of pupil dilation for frontal iris images. Wyatt,[14] an optometry researcher, conducted a very important biological analysis regarding the variations of the iris and pupil. He presented the "minimum-wear-and-tear" meshwork as a mathematical model of the iris. In addition to the nonlinear influence of the changing pupil on radial distance, he claimed that it also has an angular influence. Daugman[4] used a rubber-sheet model to show the modification of the pupil and its dimensions. Yuan and Shi[15] developed a normalization technique using linear and nonlinear methods simultaneously. Regardless of the changes in the elastic properties and muscle activities of iris, this approach has limitations. Ma et al.[16] recorded key local variation points using wavelet analysis to find the false acceptance rate resulting from pupil dilation. They showed that normalized iris images of the constricted and dilated pupils still have many differences compared with their normal state. Since the matching score between these iris images is very large, deformation-based pattern recognition approaches are proposed to address the effects of pupil dilation.[17–19] Thornton et al.[17] utilized the maximum a posteriori probability estimation parameters of relative deformation for iris matching to define the distortion-tolerant similarity metric. Wei et al.[18] used deformation correction based on Gaussian method to model the deviation from nonlinear iris stretch. Kerekes et al.[19] proposed an algorithm based on local deformation of iris patterns with a probabilistic distribution on an undirected graphical model. These studies highlighted how the pupil variations of iris images have effects on false rejection.

More recently, Hollingworth et al.[20] carried out a study on Daugman's rubber-sheet model including iris images with different dilation levels. They demonstrated that if the dilation level is the same as the compared image, the recognition of images with the small pupil is more accurate. National Institute of Standards on Technology (NIST)[21] also verified these results using a broader study on iris recognition. Ortiz et al.[22] developed an optimal strategy for dilation based iris image enrollment, where they showed a linear relationship between the matching accuracy of iris images and the variation of the pupil dilations. In addition, they found out that the most appropriate image to be recorded for matching is the one closest to the average variations of the pupil or an iris image with a pupil whose dimensions are the closest to the median dimensions. Tomeo-Reyes et al.[23] showed that dilation is not a linear process and nonlinear normalization scheme is needed to improve the accuracy of the iris recognition under different levels of pupil dilation. They proposed a biomechanical model to calculate the radial displacement of any point in the iris at a given dilation level to use it in the normalization. In summary, these studies showed that to design accurate methods for standoff iris recognition systems, researchers should address all of these challenging issues, including gaze angle and pupil dilation, simultaneously.

3 Effect of Pupil Dilation

The pupil is the opening at the center of the iris that controls the light entering the posterior eye and retina. The pupil appears to be black because light rays entering through the pupil are absorbed either directly by the retina or after reflection within the eye. Several factors affect the size of the pupil, such as the degree of retinal illumination, lens accommodation, individual's age, and also emotions.[24] While sphincter muscles encircle the pupil in the iris and contract the pupil in a circular motion, dilator muscles run radially in the iris and enlarge the pupil. Pupil dilation is a process to control the amount of incoming light through the pupil by adjusting by the iris size. In a dark environment, the pupil dilates to get more light into the eye, where its size is larger than normal ranging from 4 to 8 mm. In bright light, the pupil constricts to decrease the light amount, where its size is smaller than normal, varying from 2 to 4 mm.[25] One difficulty is that the size of the pupil changes involuntarily and pupil dilation deforms the iris texture nonlinearly.

Optical coherence tomography (OCT) is used to capture the image of the eye structures and to determine their parameters, such as thickness, height, and shape. The OCT images of the same eye with constricted and dilated irises from their vertical cross-sections are shown in Fig. 3. It is obvious that the length of the dilated iris is smaller than the constricted iris with almost the same height due to the intertwining sphincter and dilator muscles. In addition, the iris region close to the pupillary boundary is deformed more than limbus boundary.[7] Therefore, limbus occlusion becomes more severe in dilated iris images because a larger part of the iris becomes occluded in dilated images.

In traditional iris recognition algorithms, a normalization step is also used to remove the iris deformations due to the differences in pupil dilation, gaze angle, and image resolution. The majority of traditional systems use Daugman's rubber-sheet model[4] in the normalization with an assumption of a linear deformation in the iris texture. Normalization first maps the segmented circular iris pattern from Cartesian image co-ordinates to a rectangular pseudopolar co-ordinate system. This dimensionless, unwrapped image is generated

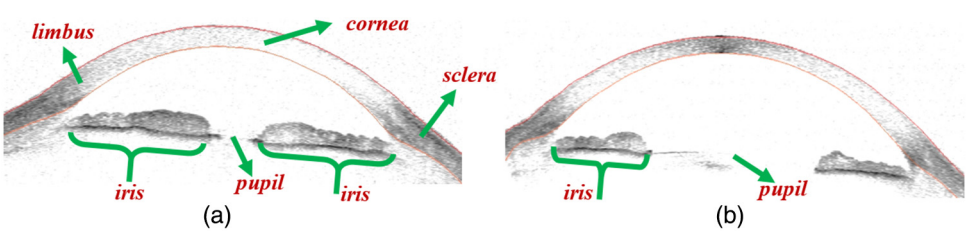

Fig. 3 OCT image of eye with (a) constricted and (b) dilated pupils.

by sampling every discrete point from the inner (pupil) to outer (sclera) boundaries. This makes all segmented irises have the same fixed size. Since the size of the pupil is determined by the iris muscles, pupil dilation generates a nonlinear deformation in the iris texture. Although the rubber-sheet model takes pupil dilation and nonconcentric pupil dislocation into account, it does not completely compensate for the nonlinear iris deformation. Furthermore, standoff systems introduce additional challenging degradation effects, including gaze angle, complex 3-D iris texture, out-of-focus blur, limbus occlusion, and illumination variations. Therefore, the rubber-sheet model is not robust enough to eliminate all challenging issues, especially in standoff systems.

In our previous study,[26] we illustrated the effect of the pupil dilation on synthetic off-angle iris images using a biometric eye model that includes the cornea, aqueous humor, limbus, iris, and sclera with their approximate geometry of eye anatomy. In order to visualize better, we first generate iris images using the eye model with circular patterns covering the 2-D iris plane at different dilation levels. Figures 4 and 5 show both frontal and off-angle images of eye models that are captured from 0 deg and 50 deg and their normalized iris images, respectively. The iris texture between inner and outer boundaries is normalized using an elliptical linear rubber-sheet model with fixed intervals.

3.1 *Pupil Dilation in Frontal Iris Images*

Figures 4(a) and 4(c) show the frontal image of a circular test pattern with different pupil dilation and their normalized images are shown in Figs. 4(b) and 4(d), respectively. Even if all circular patterns are visible in Fig. 4(a), four circles disappeared in Fig. 4(c) due to the increment on the pupil dilation. When the pupil dilates, the iris is squeezed, and its texture close to the limbus boundary is occluded by limbus. The limbus occlusion equally affects the frontal

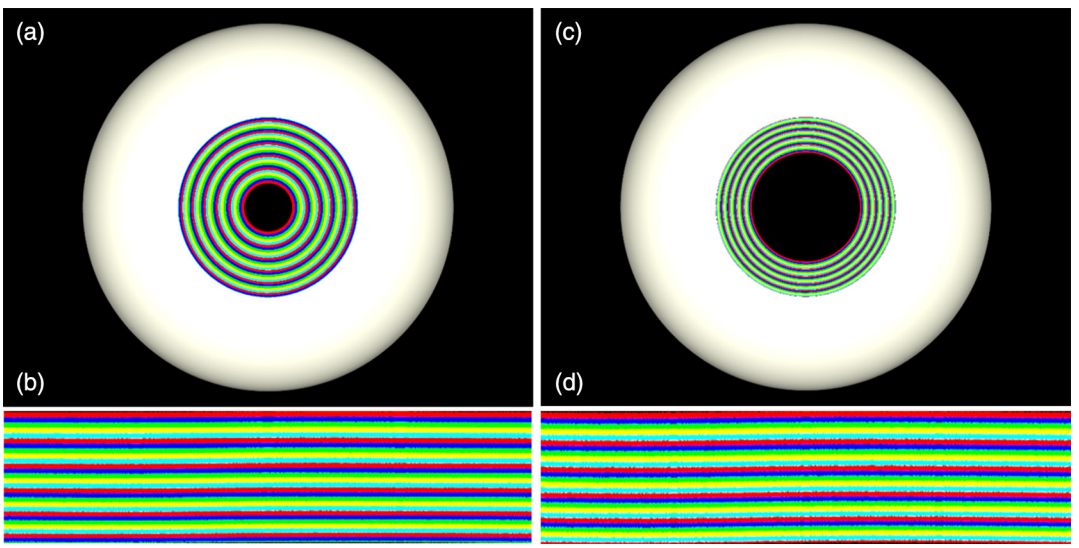

Fig. 4 (a, c) Frontal image of the eye model with circular iris texture at different dilation levels and (b, d) their normalized image using the elliptical rubber-sheet unwrapping model.

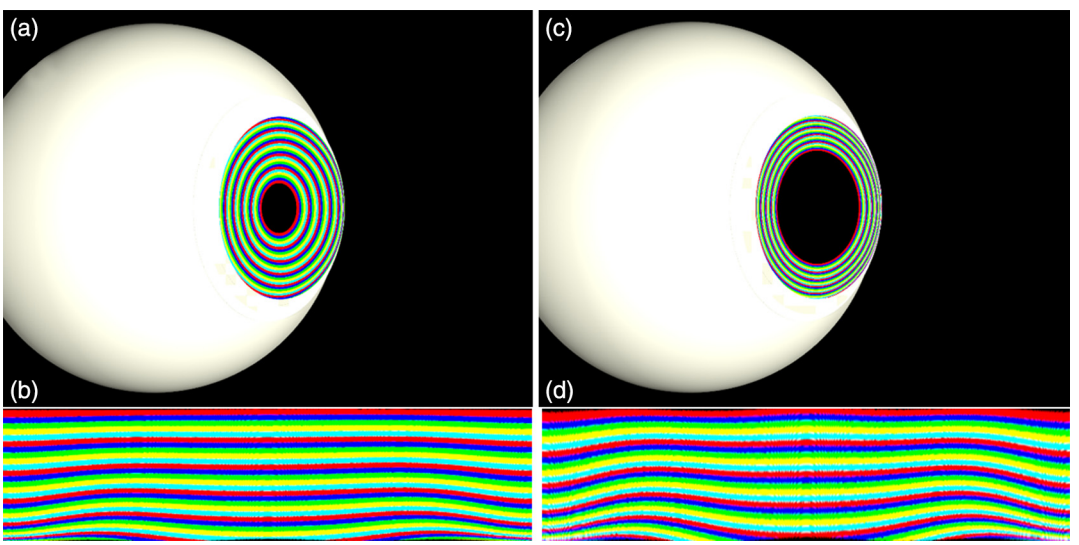

Fig. 5 (a, c) Off-angle image of the eye model with circular iris texture at different dilation levels and (b, d) their normalized image by using the elliptical rubber-sheet unwrapping model.

images by covering the same amount along the limbus boundary. This linear effect can be observed easily on normalized iris images in Figs. 4(b) and 4(d), where circular iris patterns in both images appear as nearly straight lines. Therefore, the effect of the pupil dilation on frontal iris images can be minimized by normalizing the iris images using linear rubber-sheet model. Due to the limbus occlusion, linear unwrapping cannot fully eliminate the effect of pupil dilation but it can tolerate small dilation differences between the two irises.[20]

3.2 *Pupil Dilation in Off-Angle Iris Images*

Figures 5(a) and 5(c) show off-angle iris images captured at 50 deg in angle with different dilation levels and their normalized images are shown in Figs. 5(b) and 5(d), respectively. Compared with constricted frontal iris images in Fig. 4(a), we observed that limbus occludes more iris texture on the left side than on other sides for off-angle iris images and causes optical distortion and data loss. Since limbus occlusion is uneven along the sides of the iris pattern, traditional linear unwrapping method stretched the normalized iris images differently, as shown in Fig. 5(b). When the dilation level of off-angle iris images is increased, the impact of pupil dilation on the off-angle iris images can be observed clearly in wavy normalized iris image, as shown in Fig. 5(d). These fluctuations in the appearance of iris pattern are mostly caused by the corneal refraction and limbus occlusion. The combination of the difference in gaze angle and pupil dilation causes significant distortions at circular iris patterns in the central region of the normalized off-angle iris images. Therefore, the linear rubber-sheet model is not sufficient to remove the effect of the pupil dilation in off-angle iris images. Using the traditional iris matching algorithms for these types of images generates a Hamming distance as much as within the interclass distribution. The main reasons for this dissimilarity are not only the pupil dilation and 3-D iris texture but also the corneal refraction distortion and limbus occlusion. To design an accurate off-angle iris recognition system requires considering all challenges simultaneously.

4 Experimental Setup and Dataset

To investigate the impact of pupil dilation on real off-angle iris images, we used Oak Ridge National Laboratory off-angle dilation (ORNL-OAD) dataset. This dataset contains diverse iris colors, gender groups, and ethnic backgrounds, such as Asian, African–American, and Caucasian. Among the 26 subjects, 18 are males and 8 are females. Note that even if we only focus on the pupil dilation at the off-angle images, the other challenging issues in real off-angle iris images, including 3-D iris texture, depth-of-blur, focus, and limbus effect, also influence the experimental results. This dataset has not been publicly available yet. For dataset request, researchers may contact with the Imaging, Signals, and Machine Learning Group at ORNL.

4.1 *Experimental Setup*

Our experimental setup is shown in Fig. 6. Iris images are collected by using a Toshiba Teli CleverDragon series camera and a macro lens with a telephoto converter to have a focal length of 150 mm. The camera features a 12 Mp (4096×3072) monochrome CMOS sensor with NIR sensitivity and a 25-Hz frame rate at full resolution. The iris circle diameter for a frontal iris image is around 250 pixels, where spatial resolution is 25 pixels/cm. A 720-nm long-pass filter fitted to the lens blocks ambient light while allowing most of the NIR illumination to pass. To illuminate the iris region, two M780L3-C1 collimated high-power LED infrared light sources are placed to either side of the camera facing the subjects' eye. We drive the IR light sources using T-cube LED drivers to produce constant light from 700 to 825 nm in wavelength. In addition, we placed another ambient light source next to the fixation point directed to the eye, as shown in Fig. 6(b). It is also driven using T-cube LED driver, where it produces light from 450 to 600 nm in wavelength.

By turning on and off the ambient light, we make an adjustment of the pupil dilation levels during the data capture. In order to have more accurate ground truth data, each subject is asked to place their chin into a chin rest with forehead support to keep the head stable and look ahead to a fixation point next to the camera. The subject was asked to remain steady and to keep their gaze unchanged during data capture. The camera is aligned to the corresponding eye by moving the chin rest. To capture off-angle data, the camera is placed on a moving arm, which is 50 cm in radius and can rotate from −50 deg to 50 deg in angle by a stepper motor with a constant speed. We collect data in a dark room where all lights are turned off, doors are closed, and we wait 20 s to maximize the pupil dilation. For each subject, we first move the camera to 0 deg in angle to capture frontal iris images. After starting the data capture, we first turn the ambient light on for 5 s to constrict the pupil and then we turn the ambient light off. Second, the camera is moved to 40 deg in angle to capture off-angle iris images and we repeat the same procedure in frontal data capture. For each subject, we collect around 500 frontal and 500 off-angle images from different dilation levels. Examples of frontal and off-angle iris images with different pupil dilations in the dataset are shown in Fig. 7.

After image acquisition, frontal and off-angle iris images are segmented using edge orientation based off-angle iris

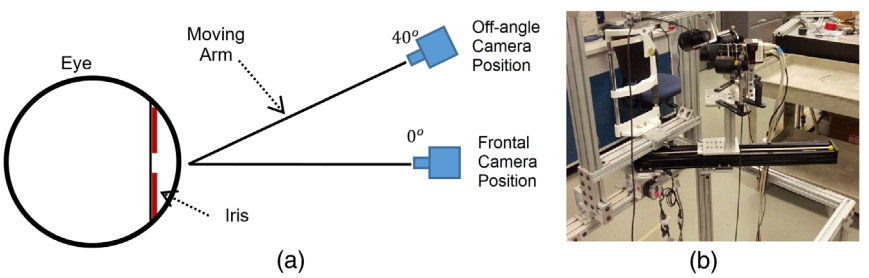

Fig. 6 (a) Illustration of experimental setup and (b) off-angle iris image data collection platform at ORNL.

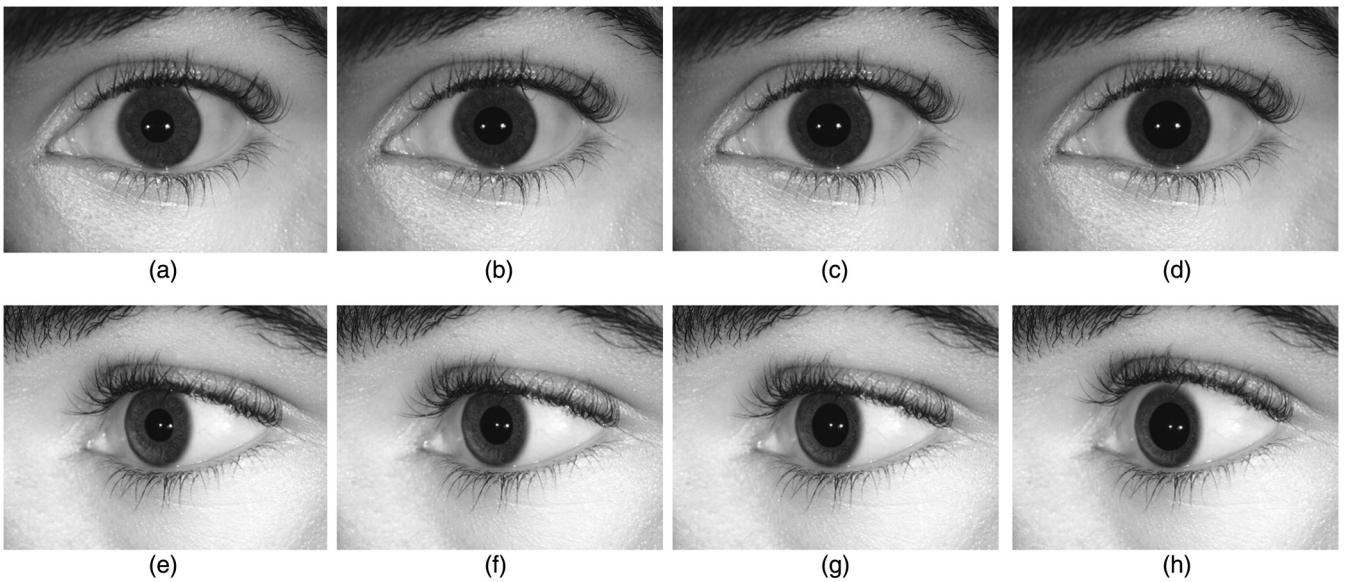

Fig. 7 Sample irises from subject s046 (a–d) frontal images from 0 deg in angle and (e–h) off-angle images from 40 deg in angle. Note that dilation levels of frontal and off-angle images are 0.41, 0.47, 0.56, and 0.60, respectively.

segmentation algorithm,[27] where pupil and iris boundaries are extracted as two ellipses. Since segmentation algorithm might introduce errors to Hamming distance calculations, we checked the segmentation results and fixed the errors using a manual ground-truth tool. This graphical user interface allows both to automatically segment the iris and to check the segmentation manually by changing the parameters. Operator checks the segmentation and fixes the error. In addition, it allows the user to detect the upper and lower eyelids by fitting second-degree polynomials. To minimize the subjective decision and to guarantee a correct segmentation, each segmentation result is checked by at least two operators. For all our experiments, we developed our programs using image processing toolbox in MATLAB 2017. The experiments are performed on a DELL Precision 7810 workstation with 8 core Xeon processor at 2.4 GHz and 16 GB memory. Computation time for segmentation, normalization, encoding, and matching per iris image is 1.5748, 0.1755, 0.0289, and 0.0247 s, respectively.

4.2 *Dataset Characteristics*

In this subsection, we present the characteristics of iris images in our dataset. We first describe the calculation of dilation levels and present the distribution of dilation levels in our frontal and off-angle iris images. Then, we adopt a well-known Gabor-based traditional iris recognition algorithm[4] to show the performance of traditional iris recognition for our dataset.

The level of pupil dilation for each iris image is measured by taking the ratio of major axes of elliptical pupil and iris segmentation parameters, as illustrated in Fig. 8. The dilation level ranges from 0 to 1, where a dilated eye has a higher value compared with a contracted eye. Since we change the amount of light coming to the eye, the pupil dilation of each subject changes over time based on the amount of light. For example, Fig. 9 shows the change in dilation levels of all collected frontal and off-angle iris images from subject s005, where it changes from 0.25 (contracted eye) to 0.54 (dilated eye). We observed that dilation level first decreased as the illumination is increased and then increased when the ambient light is turned off. Subject s005 has the biggest difference in pupil dilation level in the ORNL-OAD dataset as 0.29. This subject is convenient for analyzing with a wide range of pupil dilation levels.

The distribution of dilation levels in the ORNL-OAD dataset is shown in Fig. 10(a). In Ref. 14, the day-time dilation level for ordinary people ranges from 0.12 to 0.60. The pupil dilation levels of iris images in our dataset range from 0.16 to 0.60 for both frontal and off-angle iris images. Therefore, our dataset is consistent with the findings in

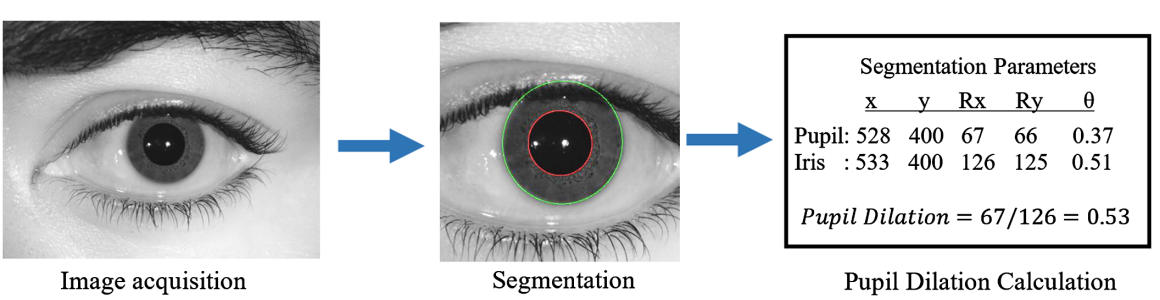

Fig. 8 Block diagram for pupil dilation calculation.

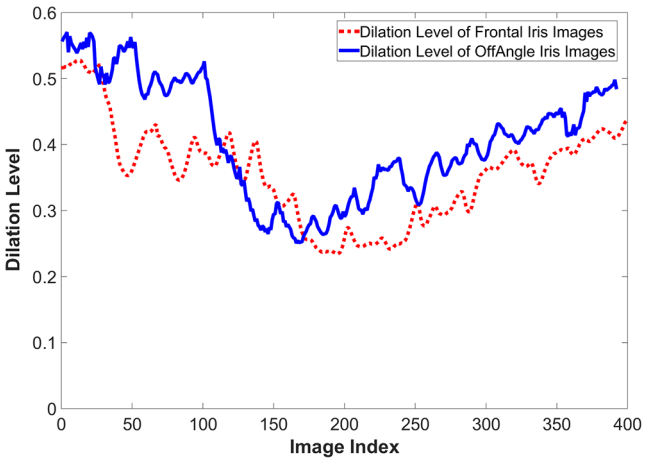

Fig. 9 Change in dilation levels of all captured frontal and off-angle iris images from subject s005.

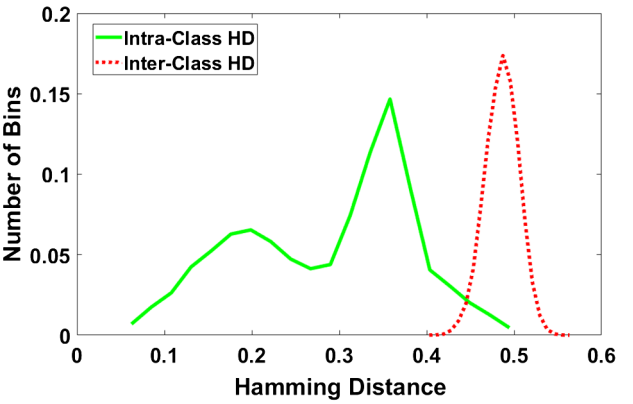

Fig. 11 Histograms of Hamming distance comparisons for each iris images in ORNL-OAD dataset.

the literature that can represent the population in daily life. We observe that the average dilation level is around 0.35 with a standard deviation of 0.1. For our experiments, we sort all frontal and off-angle iris images with respect to their dilation levels in an ascending order and select frontal and off-angle iris images that have the same dilation level. For each subject, 6 to 17 frontal and off-angle iris images are selected from different dilation levels starting from the smallest to largest with a step-size of 0.01. Figure 10(b) shows the range of dilation levels for each subject in the dataset with different colors and markers. The dilation levels of each subject vary because several factors control the pupil dilation level, including illumination, accommodation, age, and emotional conditions. For example, subject s007, the oldest subjects in our dataset, has the smallest dilation level in the dataset changing from 0.16 to 0.27, so its plot falls below others (represented by a blue solid line with + marker). Changing the amount of ambient light directed to the eye does not change the dilation level much. In addition, the subject s013 has the largest dilation level dynamic range that is represented by the longest line with a red solid line and x marker.

In order to show how the difference in gaze angle and dilation level affect the recognition performance of the traditional system, we implement the traditional iris recognition algorithm. After iris segmentation and normalization based on the elliptical inner and outer boundaries, iris codes are generated using the OSIRIS's phase-quadrant demodulation[28] to calculate the Hamming distance. Each frontal and off-angle iris image at different dilation levels is compared with each other. The comparisons between two images from the same subjects are shown in intraclass (genuine) distribution and comparisons between two different subjects generate interclass (imposter) distribution. The Hamming distance distributions of each interclass and intraclass iris comparisons in the ORNL-OAD dataset are shown in Fig. 11. The histogram on the left with a solid green line shows the distribution of iris comparisons between same subjects as intraclass Hamming distance. The distribution of interclass Hamming distance is shown on the right with a dashed red line representing the iris comparisons between two different subjects. We first observed that the intraclass Hamming distance distribution ranges from 0.06 to 0.47 with two peak points at 0.19 and 0.35. These peaks in the intraclass distribution generated due to the comparisons of iris images at same angles (frontal versus frontal and off-angle versus off-angle) and different angles (frontal versus off-angle) from the same subject, respectively. The interclass distribution ranges from 0.40 to 0.54 with a mean value of 0.48. The overlap between plots of the intraclass and

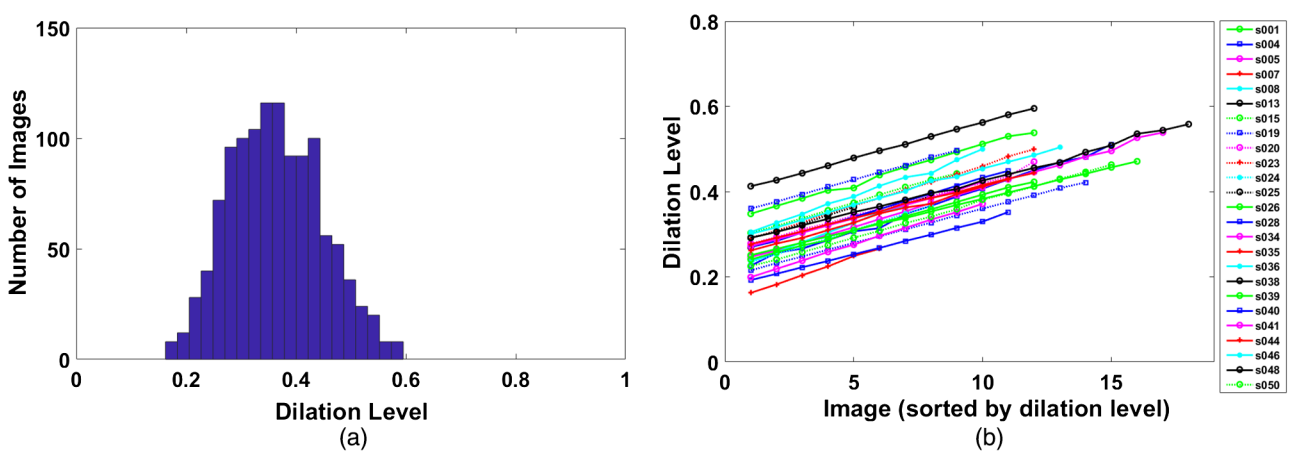

Fig. 10 The distribution of dilation levels for 26 different subjects in the ORNL-OAD dataset (a) its histogram and (b) sorted by minimum dilation ratio.

interclass distributions causes the system error (i.e., false reject and false match). In ORNL-OAD dataset, not only the gaze angle difference but also dilation level difference causes the decrement in recognition performance.

5 Results and Discussions

Although the previous section shows the combined impact on the pupil dilation and gaze angle on interclass and intraclass Hamming distribution of the ORNL-OAD dataset, it does not examine the effect of the pupil dilation and gaze angle separately on iris recognition performance. Therefore, we first group the images based on their gaze angles as frontal and off-angle with different dilation levels. Using OSIRIS's phase-quadrant demodulation, we calculate the Hamming distance between each iris image within the same subset and among the other subset. In the following subsections, we first present the effect of pupil dilation on intraclass (genuine) and interclass (imposter) distributions of frontal and off-angle iris image comparisons. Then, we summarize the effect of the pupil dilation and gaze angle on the iris recognition in a single plot using the receiver operating characteristic (ROC) curve.

5.1 *Effect of Pupil Dilation on Genuine Distributions*

Figure 12 shows the intraclass Hamming distance distributions for iris comparisons of same subjects with different dilation levels in frontal and off-angle iris subsets. The histograms from top to bottom represent the Hamming distance scores of 3316 comparisons between iris images of frontal versus frontal, off-angle versus off-angle, and frontal versus off-angle subsets, respectively. Figure 12(a) shows the Hamming distance scores of iris images in frontal subset with other images in frontal subset at different dilation

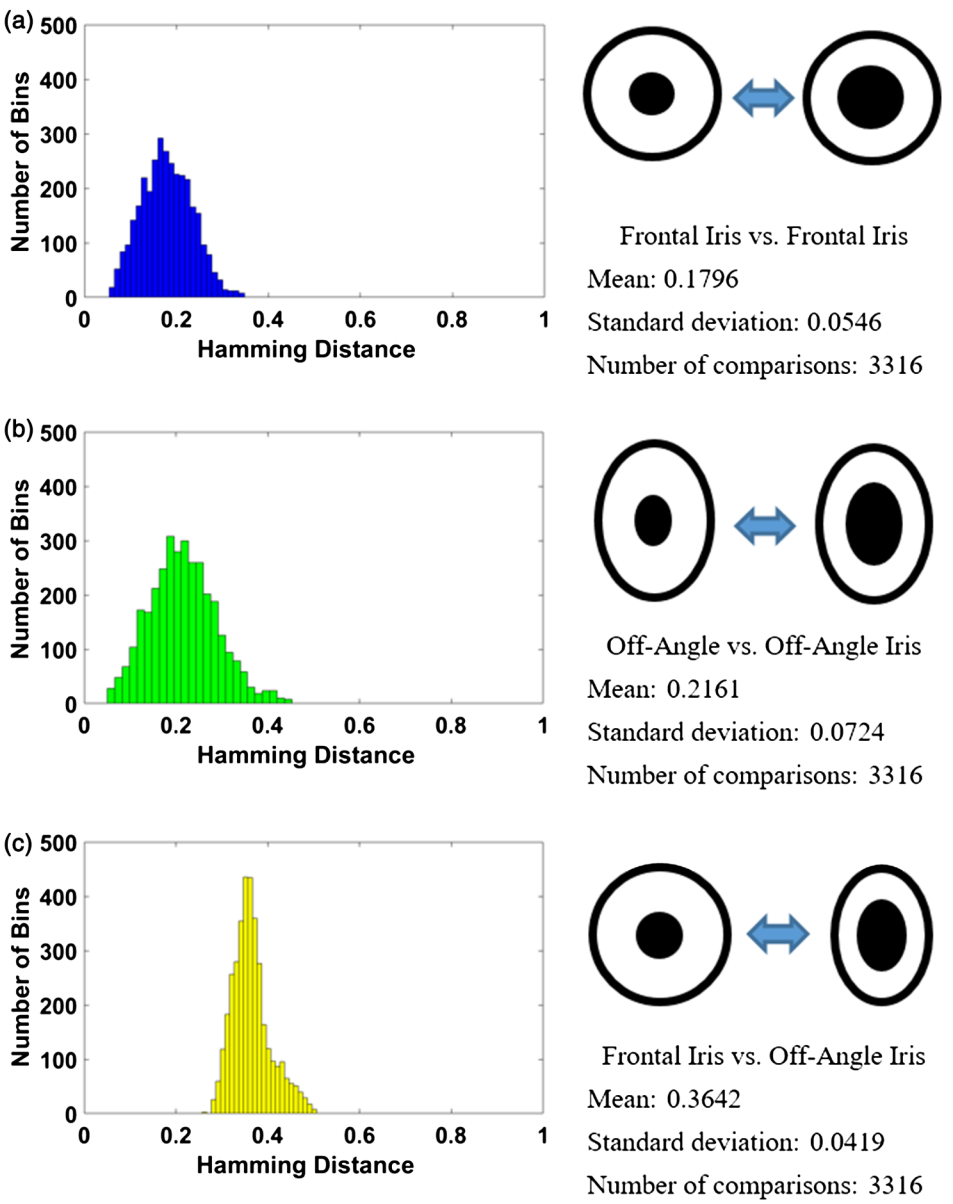

Fig. 12 Intraclass Hamming distance scores between frontal and off-angle iris images with different dilation levels (a) frontal versus frontal, (b) off-angle versus off-angle, and (c) frontal versus off-angle iris comparisons.

level. Although both images are frontal and there is no gaze difference between compared images, the distribution changes between 0.05 and 0.36 with a mean of 0.1796 and a standard deviation of 0.0546. The variation in Hamming distance is caused by the difference in dilation levels of the iris images.

Figure 12(b) shows the effect of the dilation level difference on comparison of off-angle iris images at different dilation levels. The mean of the Hamming distance scores is 0.2161 with a standard deviation of 0.0724. Since there is no gaze angle difference between compared images, we observed the similar effect with a small shift of the distribution to the right due to the severe corneal refraction of light in off-angle iris images. Since light enters the cornea almost perpendicular in frontal iris images, it is refracted almost equally at whole cornea. However, due to the gaze angle in off-angle iris images, the light is refracted at different amounts in the cornea so pupil dilation changes the location of the starting point of the iris pattern in the cornea. Therefore, the distribution of the comparison in off-angle iris images with different dilations generates slightly bigger scores.

Third distribution in Fig. 12(c) shows the Hamming distance scores from the comparison of iris images in frontal subset with images in the off-angle subset. Due to the difference in gaze angle (40 deg) and dilation level, the Hamming distance scores in frontal versus off-angle comparisons range from 0.24 to 0.47 with a mean of 0.3642 and a standard deviation of 0.0419. The combined effect of the pupil dilation and gaze angle in frontal versus off-angle comparison shifts the distribution to right compared with frontal versus frontal and off-angle versus off-angle iris comparison. These results are consistent with our previous study[7] using synthetic images, where the average Hamming distance score for the comparison of frontal and 40 deg off-angle iris images was 0.36.

In order to illustrate how dilation level differences affect iris recognition performance, we present the Hamming distance scores in the intraclass comparisons of iris images in the frontal versus frontal, off-angle versus off-angle, and frontal versus off-angle subsets. Figure 13 shows the average results of 26 subjects as mesh plots, where the dilation levels range from 0.23 to 0.53. The diagonal of the mesh plot corresponds for the comparison of the iris images at the same dilation levels, where the smallest and largest dilation levels produce the same Hamming distances. Therefore, when iris images are compared at the same dilation, the size of the pupil does not impact iris recognition performance. We observed that Hamming distance increases as the dilation level difference increases when comparing the same gaze angles (frontal versus frontal, off-angle versus off-angle), as shown in Figs. 13(a) and 13(b). The largest Hamming distance is measured for comparison of iris images that have the largest dilation difference. They are equal to 0.30 and 0.34 for frontal images and off-angle images, respectively. Hamming distance score between off-angle images is higher

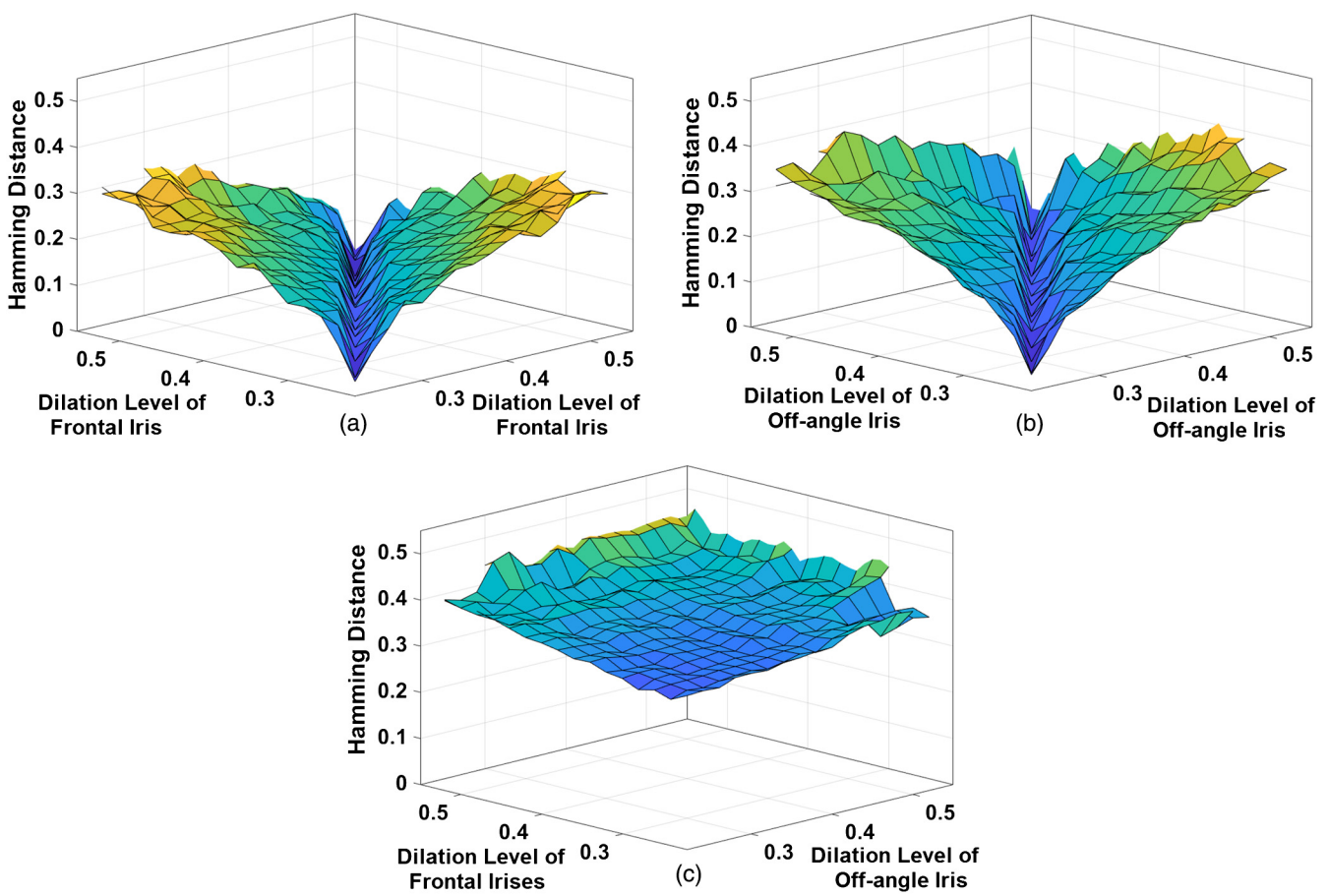

Fig. 13 Mesh plots of intraclass Hamming distance scores for (a) frontal versus frontal, (b) off-angle versus off-angle, and (c) frontal versus off-angle iris images.

than frontal images due to the more severe corneal refraction in off-angle images. The comparison of iris images from frontal versus off-angle subsets generates almost the same Hamming distance scores even if the dilation levels of compared images are different, as shown in Fig. 13(c). The Hamming distances at the diagonal of mesh plot (i.e., comparisons of images with the same dilation) have close values compared with the other regions of the mesh (i.e., comparisons of images with different dilation). This also shows that the effect of the gaze angle is the main reason for the performance degradation in off-angle iris recognition and the effect of the dilation is limited in off-angle iris images.

The effect of the pupil dilation on iris recognition with respect to the difference in the dilation level for frontal and off-angle iris images is shown in Fig. 14. Blue dashed and black dotted lines represent the comparison of frontal and off-angle iris images, respectively, at different dilation level ranging from 0.23 to 0.53, where each iris image is compared with the frontal iris image at 0.23 dilation level. We first observe that the Hamming distance increases from 0 to 0.35 as the dilation level increases from 0.23 to 0.53 in frontal iris comparison. Black solid line shows the polynomial curve fitting to the effect of pupil dilation in frontal iris images. For off-angle iris comparison, even with the same pupil dilation, Hamming distance increases to 0.35 due to the effect of the gaze angle on iris recognition performance without the dilation effect. When dilation level increases for off-angle iris images, Hamming distance increases from 0.35 to 0.40. A polynomial curve is fitted to off-angle iris comparisons shown as a blue solid line in order to visualize the effect of pupil dilation on off-angle iris images. We also observe that the result based on the experiment with real iris images agrees with the findings in simulated experiments. The increment slope in comparison of frontal iris images is larger than the off-angle iris images because the gaze angle has a significant negative effect on off-angle iris recognition performance.

These findings from real iris images are consistent with the results based on the simulated experiments in our previous study.[26] In Ref. 26, we generated synthetic iris image dataset using the biometric eye model with real iris patterns. The textures of the iris images with different dilation levels were extracted from different frontal iris images by cropping from their inner and outer boundaries. These images fed into the biometric eye model to render synthetic

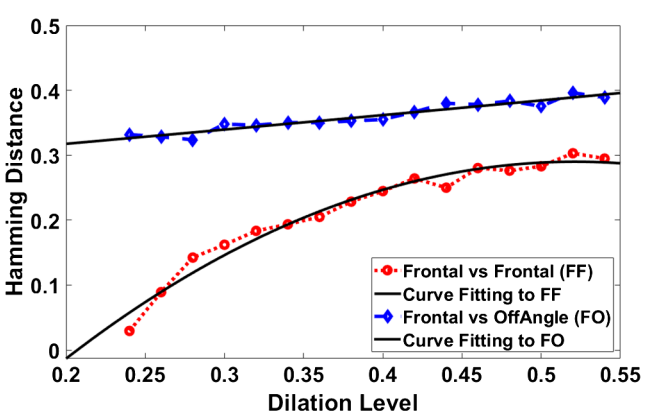

Fig. 14 Intraclass Hamming distance scores between frontal and off-angle iris images.

iris images from different angles ranging from 0 deg to 40 deg and angle and dilation levels ranging from 0.23 to 0.53 by isolating the dilation effect from other factors. In this previous work,[26] we first observed that even if image acquisition angle is fixed, all average Hamming distance scores at the intraclass distribution increase as the dilation level increases. We also observed that irises with large pupil dilation are affected more significantly from off-angle data capture, where Hamming distance between frontal and off-angle images increases by an amount ranging from 0.1 to 0.47 depending upon the pupil dilation level. This may show why the linear rubber-sheet model is not adequate to remove the effect of the pupil dilation in off-angle iris images. Compared to the iris images captured from large gaze angles, subjects with the frontal shot have better performance in off-angle iris recognition due to less corneal refraction and limbus occlusion.

5.2 *Effect of Pupil Dilation on Imposter Distributions*

The distributions of the interclass Hamming distances for iris comparisons of different subjects at different dilation levels in frontal and off-angle iris subsets are shown in Fig. 15. The histograms from top to bottom represent the Hamming distance scores of 83414 comparisons between iris images of frontal versus frontal, off-angle versus off-angle, and frontal versus off-angle subsets, respectively. We observe that the average Hamming distance scores for the interclass distributions from top to bottom are, respectively, 0.4755, 0.4704, and 0.4920 with standard deviations of 0.0267, 0.0169, and 0.0171. The decrement in the mean of the interclass distribution of off-angle versus off-angle comparison is related to the degrees of freedom in binomial distribution, where the sampling area is smaller in off-angle iris images compared with the frontal images.[7]

Figure 16 shows the intraclass and interclass Hamming distances distributions of frontal versus frontal, off-angle versus off-angle, and frontal versus off-angle subsets iris comparisons at the same plot, respectively. The largest Hamming distance is generated from the comparisons of iris images from frontal and off-angle subsets due to the gaze angle and dilation difference. Without the effect of challenging factors, including, corneal refraction, limbus occlusion, 3-D iris texture, and gaze angle in same angle iris comparisons, intraclass Hamming distance distributions are located at left compared with the comparison of irises at different angles. In order to separate the effect of the pupil dilation from the effect of gaze angle in frontal versus off-angle comparison, we also compare iris images at the same dilation level from frontal and off-angle subsets. Since both iris comparisons at frontal versus off-angle subsets with the same dilation levels and different dilation levels follow the same distributions, as shown in Fig. 16(a), the difference in the pupil dilation does not increase the Hamming distance score. Therefore, the gaze angle is the dominant effect in off-angle iris comparison compared with the pupil dilation. The effect of pupil dilation on the performance of the iris recognition system is limited when iris images compared from different angles.

5.3 *Performance Analysis Using Receiver Operating Characteristic*

To summarize the effect of the pupil dilation and gaze angle on the iris recognition in a single plot, we present the ROC

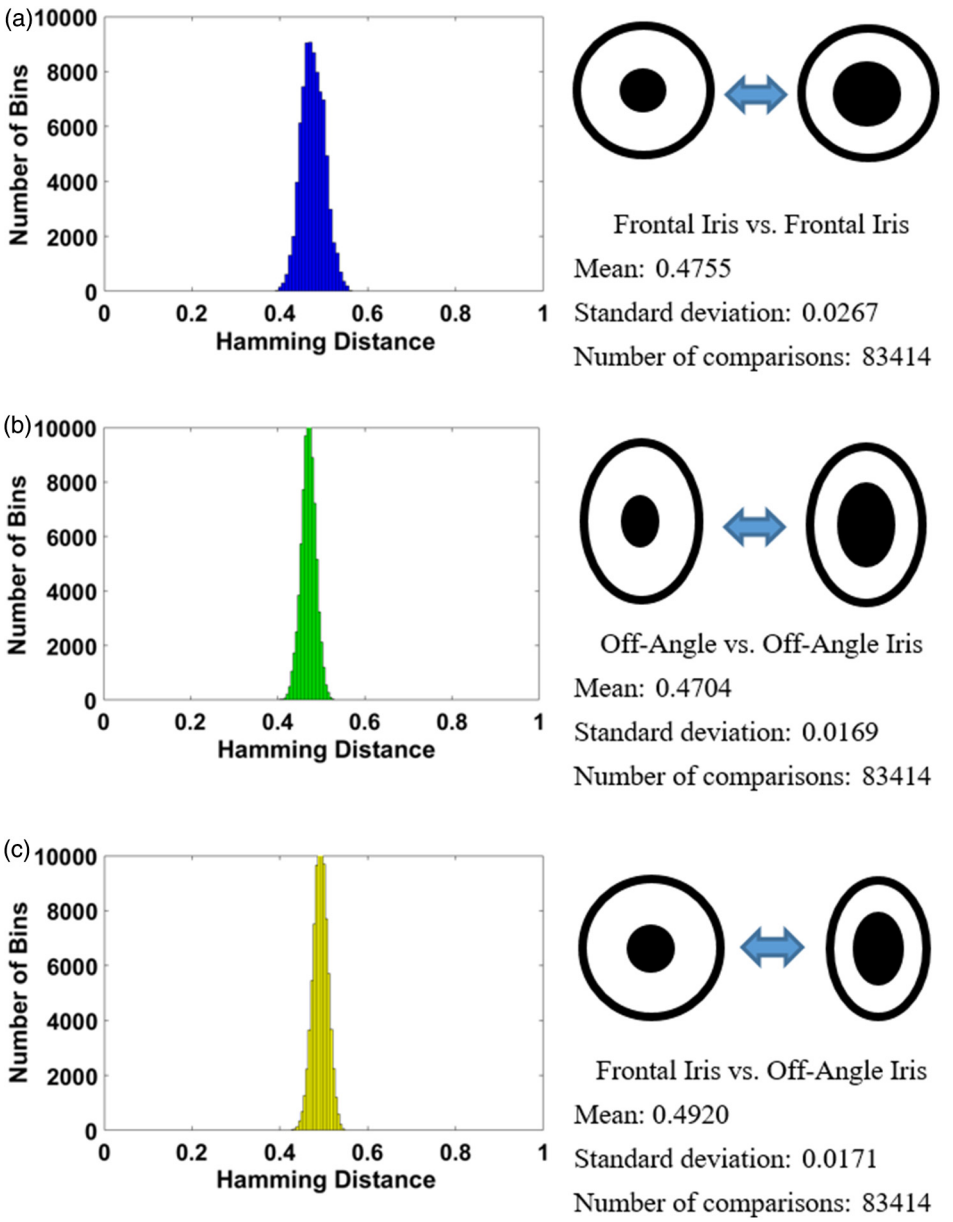

Fig. 15 Interclass Hamming distance scores between frontal and off-angle iris images with different dilation levels (a) frontal versus frontal, (b) off-angle versus off-angle, (c) frontal versus off-angle iris comparison.

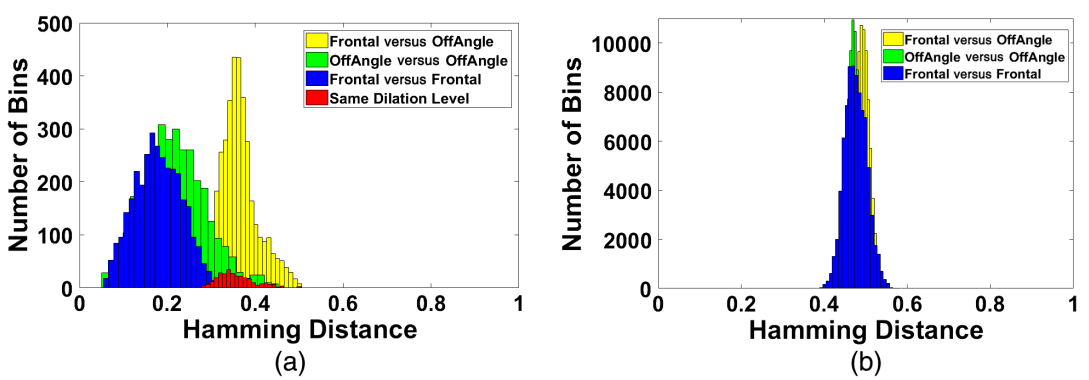

Fig. 16 Hamming distances distributions: (a) intraclass distributions of frontal versus frontal, off-angle versus off-angle and frontal versus off-angle iris comparisons at different dilation levels and frontal versus off-angle iris comparisons at same dilations. (b) Interclass distributions of frontal versus frontal, off-angle versus off-angle and frontal versus off-angle iris comparisons at different dilation levels.

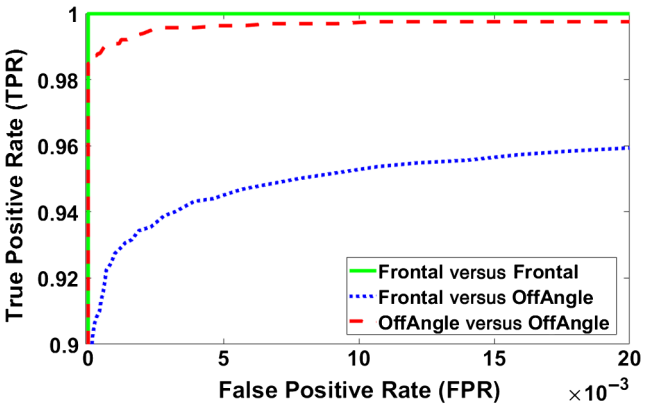

Fig. 17 Performance analysis using ROC for frontal and off-angle iris images at different dilation levels.

curve, as shown in Fig. 17. The ROC curve presents the change of the false-positive rate (FPR) and true-positive rate (TPR) in an iris recognition system by applying all possible thresholds. The minimum error rates are generated at the point that is closer to the upper left-hand corner of the graph. We generated the ROC curve for the comparison of iris images in frontal versus frontal, off-angle versus off-angle, and frontal versus off-angle subsets. Although the difference of dilation levels compared with frontal versus frontal images increases the Hamming distance scores, surprisingly, intraclass and interclass distributions do not overlap each other. Therefore, ROC curves for this subset generated the perfect separation for some threshold values without introducing errors and showed zero FPR at one TPR. That is why it shows up at the upper-left corner of the graph. However, in the literature, there are some related works[21] that reports the overlaps for the comparison of frontal iris images at different dilation levels and there exist errors in their system. Since we segment images using the elliptical segmentation and normalization methods and check the segmentation results to fix the errors, we eliminate the additional factors to increase the Hamming distance. In addition, blue dotted lines represent the ROC curve of frontal versus off-angle images that show the lowest recognition performance as expected because of the combined effect of gaze angle and pupil dilation.

Our results demonstrate that the linear rubber-sheet model can be used to eliminate the effect of the pupil dilation for the comparison of the same gaze images (frontal versus frontal and off-angle versus off-angle). However, the combination of the difference in gaze angle and dilation level causes significant distortions. Therefore, to remove the effect of pupil dilation in off-angle iris images, the linear rubber-sheet model is not sufficient. The traditional iris matching algorithms give false rejects in such cases. Main reasons are not only the pupil dilation and 3-D iris texture but also the corneal refraction distortion and limbus occlusion. Our suggestion to eliminate the effect of pupil dilation on off-angle iris images is to normalize the elliptically segmented iris images using a nonlinear sampling approach with the limbus occlusion removal masking method by considering all these challenges simultaneously.[29] The proposed approach normalizes the iris image at its actual outer boundary that is occluded by the limbus instead of the visible boundary. Since the actual outer boundary segmentation is bigger compared with the visible boundary in the traditional methods, the normalized image includes white limbus area, where limbus occludes the iris texture. To eliminate this region, we include it in the mask. The actual outer iris boundary is estimated using the relationship between actual and visible iris segmentation parameters with respect to gaze angle and limbus height. This method shows effectiveness for synthetic iris images from the biometric eye model. However, finding limbus height for each individual is a hard and nonpractical so estimation of limbus height is an open problem. To eliminate the gaze angle and pupil dilation in standoff iris recognition is possible when we accurately estimate the gaze angle and limbus height to generate the occlusion mask and nonlinear sampling pattern.

6 Conclusions and Future Work

The goal of this study was to characterize quantitatively the impact of pupil dilation on the performance of standoff iris recognition systems. We first highlighted the challenge using a biometric eye model and simulated different dilation levels and gaze angles by isolating the dilation effect from other factors. We observed that the effect of the pupil dilation on frontal iris images can be minimized by normalizing the iris images using linear rubber-sheet model. However, linear unwrapping cannot fully eliminate the effect of dilation in off-angle iris images because of not only pupil dilation and 3-D iris structures but also the corneal refraction and limbus occlusion.

In order to quantify how pupil dilation affects iris recognition performance on real off-angle images, we grouped iris images based on their gaze angles with different dilation levels and compared images in each subset with each other. We observed that the real experiment results agree with the findings in simulated experiments. Based on the real experiment results, Hamming distance increases from 0 to 0.35 as the dilation level increases. The increment slope in comparison of frontal iris images is higher than the off-angle iris images because the gaze angle has a significant negative effect on off-angle iris recognition performance. We further found that the comparison of iris images from frontal versus off-angle subsets generates almost the same Hamming distance scores even if the dilation levels of the images are different. This result shows that the effect of the gaze angle is the main reason for the performance degradation in off-angle iris recognition and the effect of the dilation is limited for steeper gaze angle. In order to design an accurate standoff iris recognition system, it is necessary to consider not only pupil dilation and 3-D iris texture but also the corneal refraction and limbus occlusion. To ignore these effects in the solution delivers a partial solution especially for iris images captured from steeper angles and subjects with larger dilation. As a future work, we will focus on finding a comprehensive solution using a realistic eye model to address all these challenges simultaneously.

Acknowledgments

This work was made possible by support from the National Science Foundation (Grant CNS-1909276) and the Research Council at University of Central Arkansas (URC-364R07).

References

1. J. Daugman, "Iris recognition at airports and border-crossings," in *Encyclopedia of Biometrics*, S. Z. Li and A. Jain, Eds., Springer, Boston, Massachusetts (2009).
2. D. M. Monro, S. Rakshit, and D. Zhang, "DCT-based iris recognition," *IEEE Trans. Pattern Anal. Mach. Intell.* **29**(4), 586–595 (2007).
3. Z. Sun and T. Tan, "Ordinal measures for iris recognition," *IEEE Trans. Pattern Anal. Mach. Intell.* **31**(12), 2211–2226 (2009).
4. J. Daugman, "How iris recognition works," *IEEE Trans. Circuits Syst. Video Technol.* **14**, 21–30 (2004).
5. J. Daugman, "New methods in iris recognition," *IEEE Trans. Syst. Man Cybern. B*, **37**(5), 1167–1175 (2007).
6. S. A. C. Schuckers et al., "On techniques for angle compensation in nonideal iris recognition," *IEEE Trans. Syst. Man Cybern.* **37**(5), 1176–1190 (2007).
7. M. Karakaya, "A study of how gaze angle affects the performance of iris recognition," *Pattern Recognit. Lett.* **82**(2), 132–143 (2016).
8. J. Zuo, N. D. Kalka, and N. A. Schmid, "A robust iris segmentation procedure for unconstrained subject presentation," in *Biom. Consortium Conf., Spec. Session Res.*, pp. 1–6 (2006).
9. X. Li et al., "A feature–level solution to off-angle iris recognition," in *Int. Conf. Biom.* (2013).
10. J. Price et al., "On the efficacy of correcting for refractive effects in iris recognition," in *IEEE Conf. Comput. Vision and Pattern Recognit.*, pp. 1–6 (2007).
11. E. Frigerio et al., "Correction method for nonideal iris recognition," in *19th IEEE Int. Conf. Image Process. (ICIP)*, pp. 1149–1152 (2012).
12. H. J. Santos-Villalobos et al., "ORNL biometric eye model for iris recognition," in *IEEE Int. Conf. Biom.: Theory Appl. And Syst. (BTAS)*, pp. 176–182 (2012).
13. M. Karakaya et al., "Limbus impact on off-angle iris degradation," in *Proc. Int. Conf. Biom.* (2013).
14. H. Wyatt, "A 'minimum-wear-tear' meshwork for the iris," *Vision Res.* **40**, 2167–2176 (2000).
15. X. Yuan and P. Shi, "A non-linear normalization model for iris recognition," in *Adv. Biom. Person Authentication*, pp. 135–141 (2005).
16. L. Ma et al., "Efficient iris recognition by characterizing key local variations," *IEEE Trans. Image Process.* **13**(6), 739–750 (2004).
17. J. Thornton, M. Savvides, and B. V. K. Vijaya Kumar, "A Bayesian approach to deformed pattern matching of images," *IEEE Trans. Pattern Anal. Mach. Intell.* **29**(4), 596–606 (2007).
18. Z. Wei, T. Tan, and Z. Sun, "Nonlinear iris deformation correction based on Gaussian model," *Lect. Notes Comput. Sci.* **4642**, 780–789 (2007).
19. R. Kerekes et al., "Graphical model approach to iris matching under deformation and occlusion," in *IEEE Int. Conf. Comput. Vision and Pattern Recognit.*, pp. 1–6 (2007).
20. K. Hollingworth, K. W. Bowyer, and P. J. Flynn, "Pupil dilation degrades iris biometric performance," *Comput. Vision Image Understanding* **113**(1), 150–157 (2009).
21. P. Grother et al., "Irex I: performance of iris recognition algorithms on standard images," *NIST Technical Report*, National Institute of Standards and Technology (2009).
22. E. Ortiz, K. Bowyer, and P. J. Flynn, "An optimal strategy for dilation based iris image enrollment," *IEEE Int. Joint Conf. Biom. (IJCB)*, pp. 1–6 (2014).
23. I. Tomeo-Reyes et al., "A biomechanical approach to iris normalization," in *Int. Conf. Biom. (ICB)*, Phuket, pp. 9–16 (2015).
24. B. Winn et al., "Factors affecting light-adapted pupil size in normal human subjects," *Invest. Ophthalmol. Vis. Sci.* **35**, 1132–1137 (1994).
25. R. H. Spector, *The Pupils Clinical Methods: The History, Physical, and Laboratory Examinations*, 3rd ed., Butterworths, Boston, Massachusetts, Chapter 58 (1990).
26. E. Celik and M. Karakaya, "Pupil dilation at synthetic off-angle iris images," in *Int. Conf. Biom. Spec. Interest Group (BIOSIG)*, Darmstadt, pp. 1–5 (2016).
27. M. Karakaya et al., "An iris segmentation algorithm based on edge orientation for off-angle iris recognition," *Proc. SPIE* **8661**, 866108 (2013).
28. E. Krichen et al., "Osiris (open source for iris) reference system," BioSecure Project, http://www.biosecure.info (2008).
29. O. M. Kurtuncu and M. Karakaya, "Limbus impact removal for off-angle iris recognition using eye models," in *7th IEEE Int. Conf. Biom.: Theory, Appl. and Syst.*, Washington DC (2015).

Mahmut Karakaya is an assistant professor at the University of Central Arkansas. He received his BS degree in 2005, MS degree in electrical engineering from the University of South Alabama in 2007, and PhD degree in computer engineering from the University of Tennessee in 2011. He is the author of more than 30 articles and holds two patents. His research interests include digital image processing, smart camera networks, and iris recognition. He is a member of SPIE.

Elif T. Celik received a BS degree in computer engineering from Gazi University in 1995 and a PhD from Polytechnic University, Bucharest, Romania, in 2012. Her research interests are in the area of image processing and biometrics.